IEEE Photonics Journal
An IEEE Photonics Society Publication

Open Access

Quasiperiodic Dielectric Gratings for Multiband Fiber-To-Chip Couplers

Volume 12, Number 5, October 2020

Odair J. Picin
Faustino Reyes Gómez
Ernesto Reyes-Gómez
Osvaldo N. Oliveira Jr
J. Ricardo Mejía-Salazar

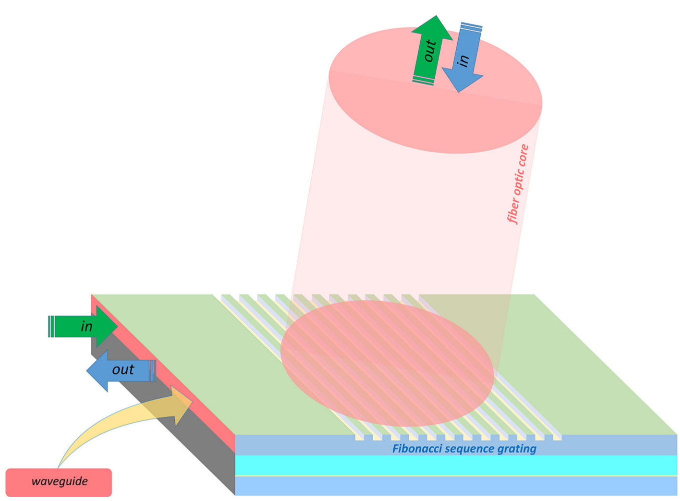

DOI: 10.1109/JPHOT.2020.3029025

IEEE photonics SOCIETY
IEEE

Quasiperiodic Dielectric Gratings for Multiband Fiber-To-Chip Couplers

Odair J. Picin,[1] **Faustino Reyes Gómez,**[2] **Ernesto Reyes-Gómez,**[3] **Osvaldo N. Oliveira Jr**,[2] **and J. Ricardo Mejía-Salazar**[1]

[1]National Institute of Telecommunications (Inatel), 37540-000 Santa Rita do Sapucaí, Brazil
[2]São Carlos Institute of Physics, University of São Paulo, 13560-970 São Carlos, Brazil
[3]Instituto de Física, Universidad de Antioquia, Medellín 050010, Colombia

DOI:10.1109/JPHOT.2020.3029025

Manuscript received August 3, 2020; revised September 28, 2020; accepted October 1, 2020. Date of publication October 7, 2020; date of current version October 16, 2020. This work was supported in part by the National Council for Scientific and Technological Development - CNPq under Grants 305958/2018-6 and 429496/2018-4, in part by FAPESP under Grant 2018/22214-6, in part by RNP, with resources from MCTIC, under Grant 01250.075413/2018-04, through the Radiocommunication Reference Center (Centro de Referência em Radiocomunicações - CRR) project of the National Institute of Telecommunications (Instituto Nacional de Telecomunicações - Inatel), Brazil. The work of E. R.-G. was supported by Scientific Colombian Agency CODI-University of Antioquia. Corresponding author: J. Ricardo Mejía-Salazar. (e-mail: jrmejia@inatel.br).
This article has supplementary downloadable material available at https://ieeexplore.ieee.org, provided by the authors.

Abstract: Dielectric gratings that couple optical fibers and planar waveguide circuits are key for optical-to-electronic (electronic-to-optical) signal conversion, but their applicability to platforms that require broader bandwidths and higher capacity is limited by their single-wavelength response. Herein, we present the design of a quasi-periodic grating coupler with multiband fiber-to-waveguide (waveguide-to-fiber) coupling response, where the grating consists of a periodic repetition of unit cells made of alternating silicon and air grooves according to the Fibonacci sequence. Through finite-difference time-domain (FDTD) calculations, we show that this new device could be used for coupling multi-wavelength fiber modes in a single grating structure. The results were obtained for fibers operating in the wavelength range from 1000 nm to 2000 nm, but the concept can be readily extended to other frequency ranges. Moreover, the allowed modes in the grating are almost insensitive to fiber misalignments and small fabrication errors for high Fibonacci steps, which is useful when alignment of optical components is impractical. It is hoped that properly designed gratings overlapping multiple modes may lead to ultra-broadband fiber-waveguide couplers that can cope with the growing demand for higher capacity and bandwidth in optical communications.

Index Terms: Grating-couplers, quasiperiodic, fiber-to-chip coupling.

I. Introduction

The seamless integration of fibre-optics networks with photonic integrated circuits (PIC) and microelectronic devices may fulfill the ever growing demand for higher data rates in optical communications [1], [2]. This convergence of optical and electronics, mediated by photonic technologies, has stimulated research into various directions, as in the coupling of optical-to-electronic or electronic-to-optical signals (optoelectronics) through dielectric semiconducting periodic grating couplers [2]–[9]. Research has been mostly focused on periodic or apodized grating systems which produce high efficiencies but have limited operation bandwidths. For instance, periodic dielectric grating structures have been explored for efficient chip-to-fiber (fiber-to-chip) coupling [10], [11], and now there is renewed interest because of their unique ability for high-density PIC [12]–[17]. Recent approaches for grating-couplers include the use of metamaterials and backside metal mirrors to improve coupling efficiency [18], [19]. However, the very narrow operational wavelength range owing to the dispersive working principle constitutes a major hurdle for multichannel high performance communication [6], [15]. This drawback needs to be circumvented to enable future PICs with many optical input-outputs [2], [20], like frequency-comb generation or wavelength-division multiplexing [21]. Some attempts include the design of subwavelength grating edge couplers [5]–[7], [9], two-dimensional periodic arrays [4] and the use of gradient-based inverse design approaches [22]. Coupling efficiencies in grating-based couplers depend strongly on the phase-matching condition, $k_0 n_{\rm eff} - k_0 n_{\rm c} \sin\theta = G_p$, where $k_0 = \frac{2\pi}{\lambda}$, $n_{\rm c} = 1.0$ is the refractive index of the cladding material (air in this case), $n_{\rm eff}$ is the effective refractive index (RI) for the optical mode, θ is the incident angle, and G_p is the reciprocal lattice vector. This mechanism is used to produce grating couplers working around a specific wavelength. Broadband grating platforms have been designed with two-dimensional apodized [17] and focusing-curved [5] structures. Although these systems can be developed with standard industrial tools to exhibit 1-dB bandwidths up to around 130 nm, their coupling efficiencies are conventionally lower than 30%.

The broadband capability of quasiperiodic gratings, i.e., self-similar structures, on the other hand, has not been explored for efficient broadband coupling interfaces between a chip and optical fibers. Here we present such a study with the design of a grating coupler with multiple reciprocal wave vectors from quasiperiodic systems for broadband fiber-to-chip (chip-to-fiber) coupling. Analogous systems have been employed for light trapping in photovoltaics [23], broadband enhancement of second harmonic generation [24]–[26], reduction in the light beam expansion in quasi-periodic waveguide arrays [25], and for broadband-enhanced magnetoplasmonic effects [27]. We considered the gratings made as a periodic repetition of quasi-periodic elementary cells (F_m) patterned along the z-axis. The building blocks of these elementary cells, A (silicon) and B (air), were alternated according to the $m-$th step of the Fibonacci sequence [26], [28], obtained from the inflation law $F_m(A, B) = F_{m-1}(A, B)|F_{m-2}(A, B)$, for $m \geq 2$, with the initial conditions $F_0(A, B) = B$, $F_1(A, B) = A$ and the symbol "|" indicating a concatenation operation. Unit cells for F_2, F_3 and F_4 are schematized in Figure 1(a). The total number N_m of A and B blocks in the elementary cell F_m follows the Fibonacci succession $N_m = N_{m-1} + N_{m-2}$, with $N_0 = N_1 = 1$. The length L_m of the elementary cell F_m is given by $L_m = N_{m-1}a + N_{m-2}b$, where $a = 315$ nm and $b = 315$ nm are the lengths of the building blocks A and B, respectively. The reciprocal wave vectors for the phase-matching condition becomes now a set $G_{p,m}$, where the index m must be used to indicate its dependence on the Fibonacci-step followed by the unit cell. Figure 1(b) shows a xy-plane view of the fiber-grating alignment ($\phi = 0^\circ$ in this work). All the simulations were performed with the commercial software Lumerical FDTD, already used in the study of periodic grating couplers [12], [17], [18]. The simulation setup in the Lumerical software is schematized in Figure 1(c) for F_2, where the grating and waveguide (for each F_m) were considered as made of Si on SiO_2, with a bottom Au/Si mirror to improve the coupling efficiencies. The grating-fiber distance d affects the coupling efficiency strongly [3]. Through an automatized algorithm to optimize the coupling efficiency of the structure, we obtained different d values for each tilt-angle of the fiber. We used $d = 0.78$ μm for $\theta = 6^\circ$ and $\theta = 7^\circ$; for $\theta = 8^\circ$ and $\theta = 11^\circ$ we used $d = 0.79$ μm, whereas for $\theta = 12^\circ$ and $\theta = 14^\circ$ we used $d = 0.8$ μm. Two ports at the fiber-grating *i)* and at the grating-waveguide *ii)* interfaces were used to measure the coupling efficiencies in the wavelength range of interest. These ports were configured to work in the fundamental mode of the grating, i.e., for $p = 1$.

II. Design of Grating Couplers and Self-Similarity Effects

We focus on gratings for waveguide to/from fiber-optic coupling at multiple working wavelengths, particularly from $\lambda = 1000$ nm to $\lambda = 2000$ nm. The waveguide thickness can be changed to improve the coupling efficiencies, but we fixed to 220 nm for simplicity and because this value

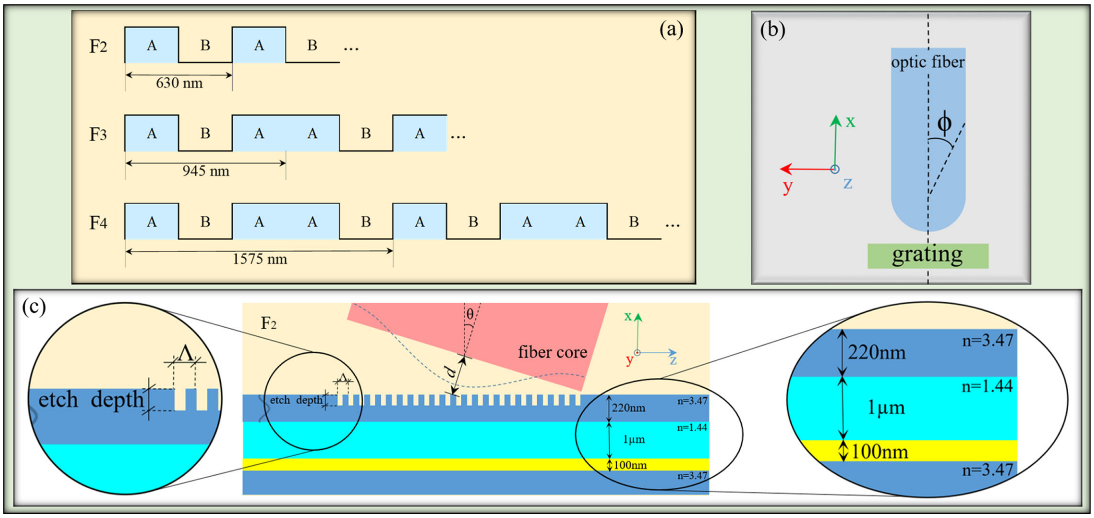

Fig. 1. (a) Schematics of period lengths and composition for the Fibonacci steps $m = 2$, $m = 3$, and $m = 4$. (b) Side-view of the fiber-grating system showing the alignment used in this work, $\phi = 0$. (c) xz-plane side-view schematic of F_2 (periodic) grating-coupler, with a 0.1 μm bottom-gold mirror layer and a top cladding layer of air ($n_c = 1.0$). The slab thicknesses and refractive indices of the corresponding silicon ($n = 3.47$) and glass ($n = 1.44$) layers are shown. The period length (Λ), fiber core, distance between fiber and grating (d) and the fiber-tilt angle (θ) are also illustrated.

is a common standard in industry [14], [16], [29] for $\lambda = 1550$ nm (our central wavelength). The number or periods for each F_m decreases with m to have the total grating length below 17 μm. More specifically, we used 24, 16, 10, and 6 periods for $m = 2$, 3, 4, and 5, respectively. Coupling efficiencies for F_2, F_3, F_4 and F_5 are shown in Figure 2 for different θ and etch-depths. Figures 2(a) and 2(b) are for $\theta = 6^\circ$ and $\theta = 10^\circ$, respectively, with an $etch - depth = 70$ nm, whilst Figures 2(c) and 2(d) are for etch-depths of 110 nm and 140 nm, respectively, with $\theta = 10^\circ$. The maximum efficiencies are modulated by the corresponding etch-depths and θ, as expected [14], [30]. In general, the light field along the patterning direction can be expressed as [31]

$$E(z) = E_0 e^{ik_0 z \sin\theta} \sum_{p=0}^{\infty} A_{p,m} e^{iG_{p,m} z}, \tag{1}$$

where $A_{p,m}$ is the amplitude of the p-th diffraction order, and $G_{p,m}$ are found from the Fourier transform of the grating-pattern. As the silicon and air blocks have the same widths for each m, and the coordinates in the reciprocal space ($G_{p,m}$) appear as peaks in the Fourier spectra (allowed modes), a correlation among the reciprocal lattices is expected. This correlation results in a successive splitting of each photonic quasi-band around $G_{p,2}$ as m increases [26], [27], [28]. In other words, multiple coupling-efficiency peaks in quasiperiodic structures (in contrast to periodic ones) result from the loss of long-range spatial coherence of the electromagnetic field along the patterning direction [28]. Poorly-defined peaks for F_5 are due to the lack of periodic features because of the small number of unit cells (6) for $m = 5$. As already mentioned, the aim in this work is to demonstrate the possible use of quasiperiodic gratings for multiple high efficiency peaks within a desired frequency range, i.e., geometrical parameters and the number of periods can be optimized for improved efficiencies [14], [32]. Since gratings for each m-th Fibonacci-step exhibit the same results for fiber-to-waveguide (in-coupling) and waveguide-to-fiber (out-coupling) coupling efficiencies, we will address coupling efficiencies without any reference as to whether they are in-coupling or out-coupling devices.

Figure 3 shows the 1-dB bandwidth for some of the coupling efficiency peaks in Figure 2. We observed a 1-dB bandwidth of 49 nm for F_2 in Figure 2(a) (see Figure 3(a)). For F_4 from Figure 2(c),

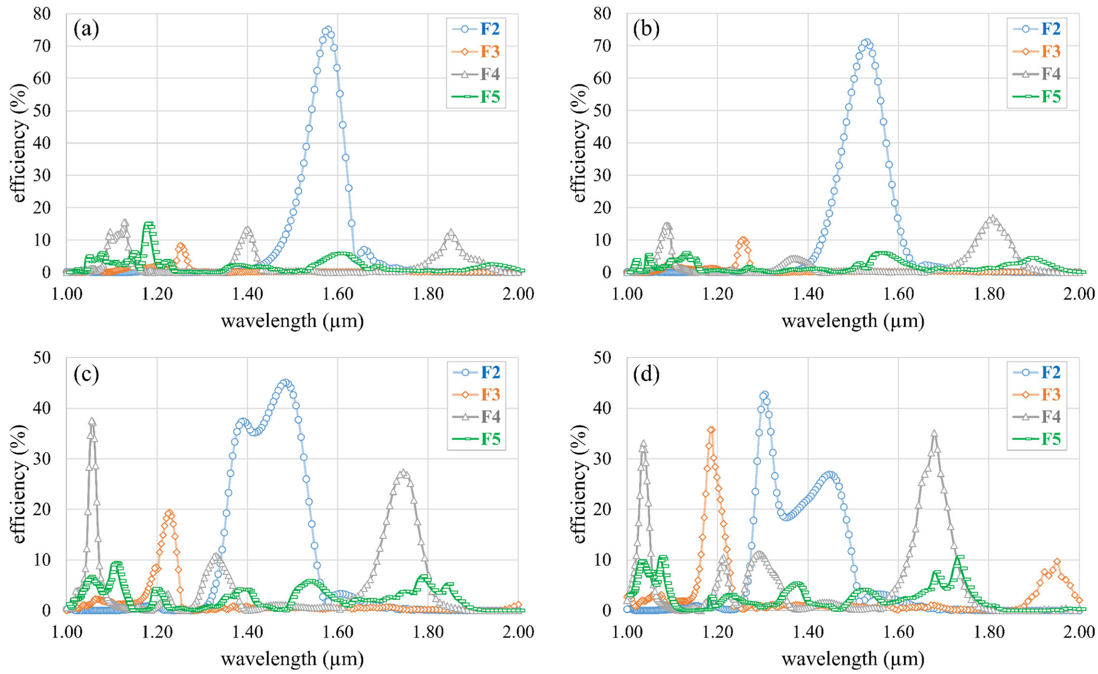

Fig. 2. Light coupling efficiencies for grating structures with unit cells F_2, F_3, F_4, and F_5 with an $\text{etch}-\text{depth} = 70$ nm for (a) $\theta = 6^\circ$ and (b) $\theta = 10^\circ$. Results for $\theta = 10^\circ$ with different etch-depths are also plotted for (c) $\text{etch}-\text{depth} = 110$ nm and (d) $\text{etch}-\text{depth} = 140$ nm.

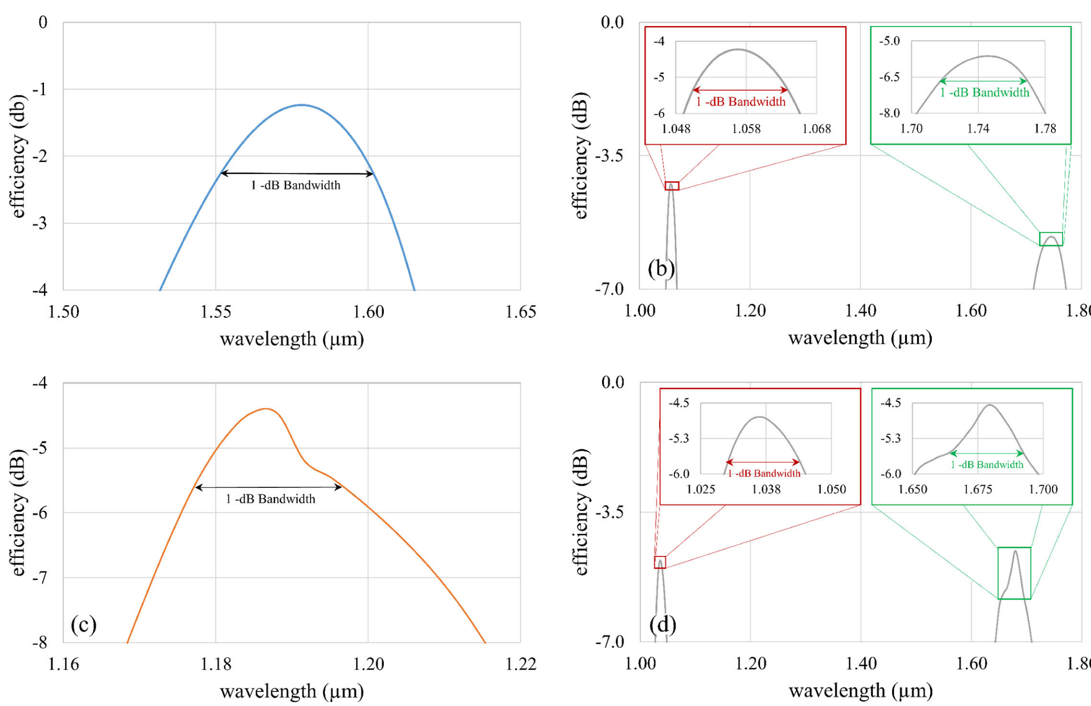

Fig. 3. Light coupling efficiencies with the corresponding 1-dB bandwidths for grating structures with unit cells F_2, F_3, and F_4. Results are for (a) F_2 with $\theta = 6^\circ$ and $\text{etch}-\text{depth} = 70$ nm, (b) F_4 for $\theta = 10^\circ$ and $\text{etch}-\text{depth} = 110$ nm, (c) F_3 for $\theta = 10^\circ$ and $\text{etch}-\text{depth} = 140$ nm and (d) F_4 for $\theta = 10^\circ$ and $\text{etch}-\text{depth} = 140$ nm.

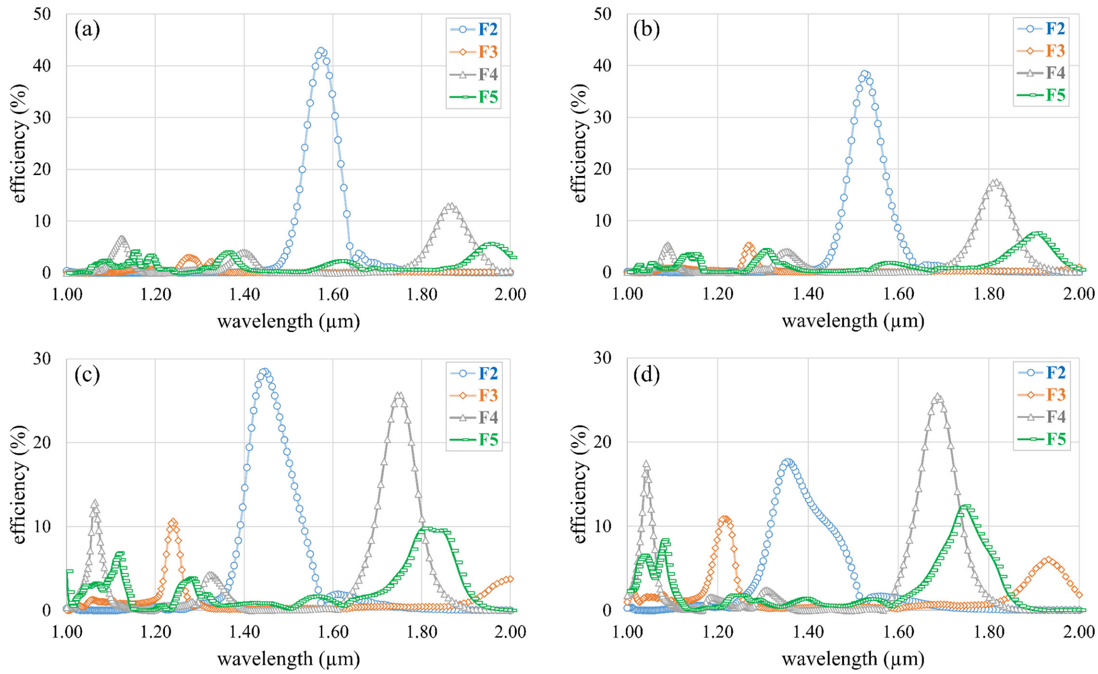

Fig. 4. Light coupling efficiencies for grating structures without the bottom-gold mirror layer, with unit cells F_2, F_3, F_4, and F_5 with an etch − depth = 70 nm for (a) $\theta = 6^\circ$ and (b) $\theta = 10^\circ$. Results for $\theta = 10^\circ$ with different etch-depths are also plotted for (c) etch − depth = 110 nm and (d) etch − depth = 140 nm.

there are 1-dB bandwidths of 14 nm and 50 nm for the peaks at $\lambda_{\text{peak}} = 1056$ nm and $\lambda_{\text{peak}} = 1746$ nm, respectively, as seen in Figure 3(b). As for F_3 in Figure 2(d), there is a 1-dB bandwidth of 17 nm. Figure 3(d) shows 1-dB bandwidths of 15 nm (for $\lambda_{\text{peak}} = 1036$ nm) and 25 nm (for $\lambda_{\text{peak}} = 1679$ nm) for F_4 from Figure 2(d). One notes that the etch − depth not only affects the peak position but also the corresponding bandwidth.

In order to estimate the contribution from the bottom-gold mirror layer, we calculated the corresponding coupling efficiencies for the systems in Figure 2 without this metallic layer. The results in Figure 4 indicate a drop in the efficiency peaks for all Fibonacci steps considered here. Only for the case of F_5 in Figure 4(d) does one note that the coupling efficiency remains around 10%, which may be due to the dominant reflective behavior at the fiber-grating interface.

III. Tilt-Angle and Etch-Depth Dependent Maximum Efficiencies

Calculations of the maximum coupling efficiencies, and their corresponding wavelengths, were performed as functions of the tilt-angle and etch-depth for each F_m structure. Results for $m = 2$, 3, and 4, are shown in Figures 5, 6, and 7, respectively. Multiple coupling efficiency (CE) peaks exist for F_3 and F_4, but only the highest are shown. In fact, F_4 has two similar high CE peaks with wavelengths $\lambda = 1.04$ μm (CE = 33.13%) and $\lambda = 1.68$ μm (CE = 35.12%), and two low CE peaks around $\lambda = 1.21$ μm (CE = 10.45%) and $\lambda = 1.29$ μm (CE = 11.24%), for etch − depth = 140 nm and $\theta = 10^\circ$, as observed from Figure 2 d. The highest CE peaks (the associated wavelengths) are shown as functions of θ and etch-depth in Figure 5 for the periodic system F_2. Numerical results are presented for different etch-depths and θ values in Figures 5 a and 5 b (5 c and 5 d), respectively. Simulations were performed for a total grating length of 15.12 μm, corresponding to 24 repetitions of the unit cell AB (630 nm period length). The waveguide and the end of the grating coupler were 12.3 μm and 1.88 μm long, respectively, for a total lateral length of 29.3 μm for the calculation

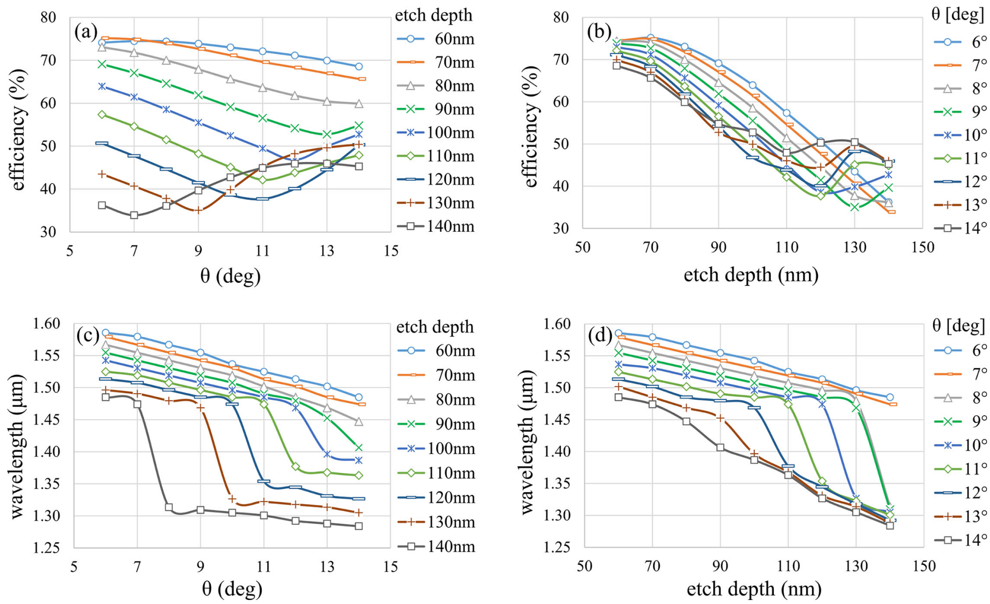

Fig. 5. Highest coupling efficiency for the F_2 system consisting in the repetition of 24 periods *AB*, as a function of a) fiber's tilt-angle and b) groove etch-depth. c) and d) show the wavelengths associated with these coupling efficiency peaks as a function of the the fiber's tilt-angle and groove etch-depth, respectively. Small losses for $\theta = 6^\circ$ and $\mathrm{etch}-\mathrm{depth} = 70$ nm in a) are mainly due to undesired reflections at the grating-fiber interface (see **Visualization 1**).

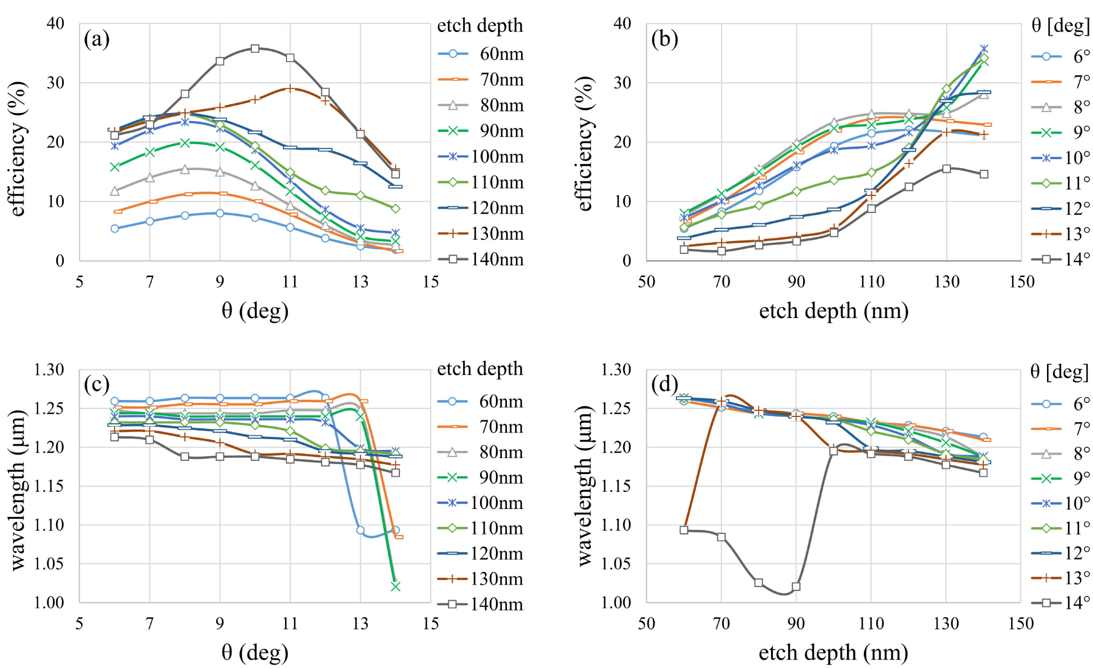

Fig. 6. Highest coupling efficiency for the F_3 system made with repetition of 16 *ABA* periods, as function of a) the fiber's tilt-angle and b) the groove etch-depth. c) and d) show the wavelength associated to these coupling efficiency peaks as a function of the the fiber's tilt-angle and the groove etch-depth, respectively. In contrast to F_2, the highest CE peak for this system (with $\theta = 10^\circ$ and $\mathrm{etch}-\mathrm{depth} = 140$ nm) is lower due to reflections at the grating-fiber interface and light guiding in the glass below the Si waveguide (see **Visualization 2**).

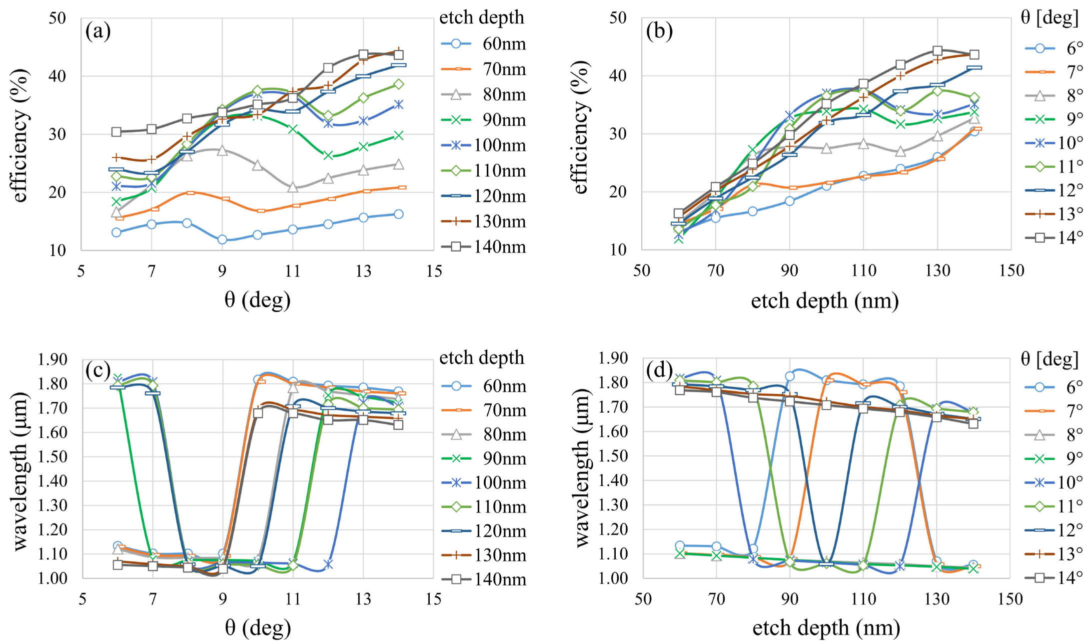

Fig. 7. Highest coupling efficiency for the F_4 system made with repetition of 10 *ABAAB* periods, as function of a) fiber's tilt-angle and b) groove etch-depth. c) and d) show the wavelengths associated with these coupling efficiency peaks as a function of fiber's tilt-angle and groove etch-depth, respectively. Lower CE peaks, in comparison to F_2, are due to higher reflections at the grating-fiber interface and light guiding in the glass below the Si waveguide, as it can be appreciated from **Visualization 3**.

domain. The other geometrical and material parameters described in the previous sections were taken as the same for all the systems in this work. The electric field was considered polarized along the *y*-direction, with reference to Figure 1 c, in order to excite the transverse electric (TE) field mode of the integrated waveguide. The maximum CE and their associated wavelength are observed to be little sensitive to the fiber's tilt-angle for an etch depth of 60 nm. In contrast, CE exhibits a rapid decaying behavior for etch-depths above 70 nm for all θ values. Recent works [13], [32] indicated that the CE dependence on the etch-depth can be controlled through the waveguide thickness, which in the present work we consider fixed to 220 nm. Analogous results are shown for F_3 and F_4 in Figures 6 and 7. Numerical simulations were carried out for F_3 and a grating coupler made with 16 *ABA* periods, with a total length of 15.12 μm. The waveguide and the end of the grating coupler have the same lengths as for F_2. In the case of F_4 we used a grating with a length of 15.75 μm, corresponding to 10 periods *ABAAB*. The waveguide length and the end of the grating were considered as 12.3 μm and 1.25 μm, respectively. In contrast to the results for F_2, we must note that resonant wavelengths become less sensitive to changes in θ and etch-depth as *m* increases, i.e., CE wavelength-peaks (not their amplitudes) are robust to small variations in the fabrication process and fiber-misalignments. We stress that several CE peaks were observed for the non-optimized F_3 and F_4 systems, whereas the results in Figures 6 and 7 only show the highest CE peaks to emphasize the maximum efficiency dependence on the θ and etch-depth parameters. Lower CE amplitudes for F_3 (see **Visualization 2**) and F_4 (see **Visualization 3**) in comparison to F_2 (see **Visualization 1**) are due to the higher reflection at the grating interface and to the light guiding in the glass below the Si waveguide, as it can be appreciated from FDTD videos in the visualization files. These reflections are mainly due to the excitation of higher order modes for incident angles larger than 8°. From these results we expect that higher CE values with high tolerance to fabrication errors will be reached through proper optimization methods for grating couplers [14] and thicker Si waveguides [13], [32]. The proper engineering of an index matching period at the beginning of

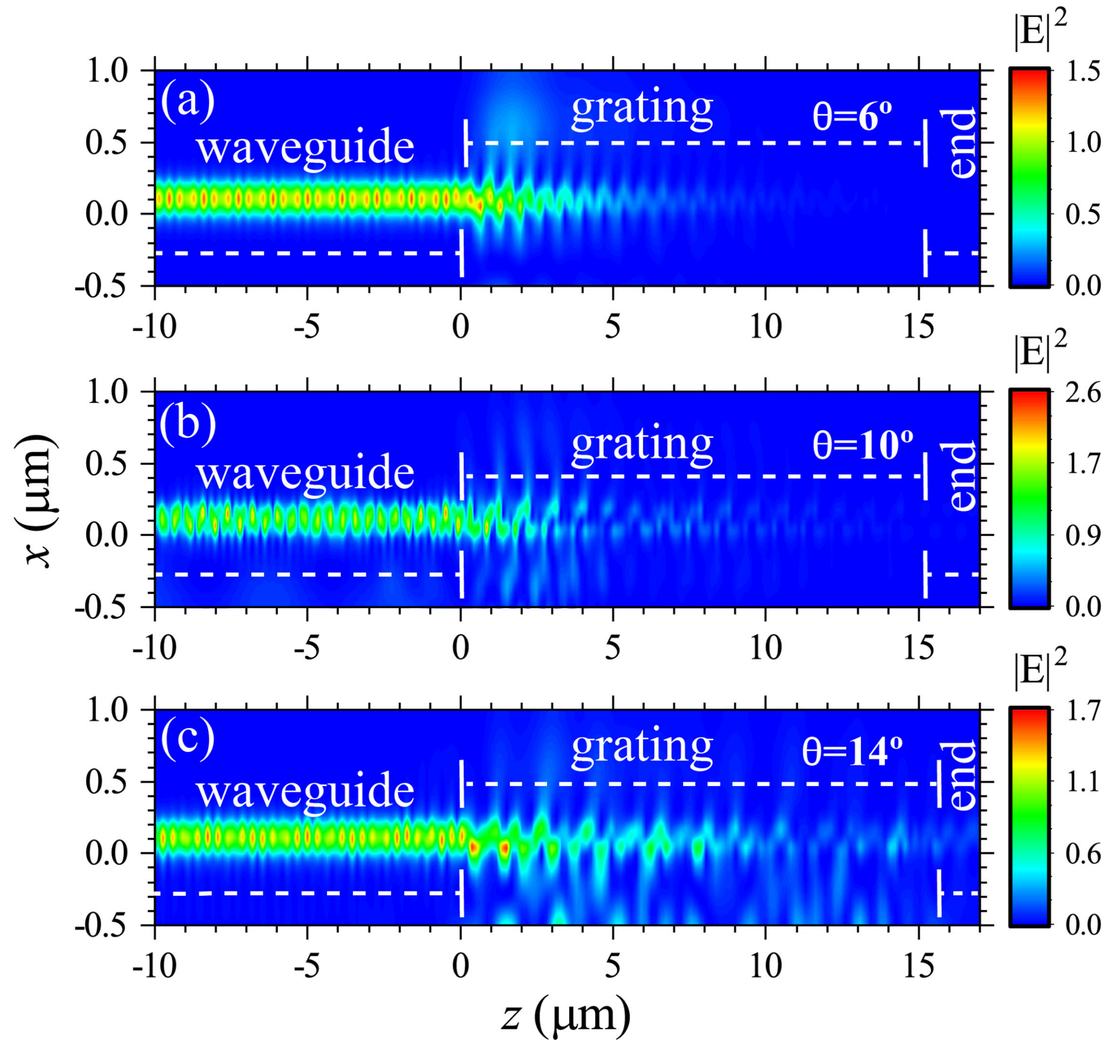

Fig. 8. Field profiles associated with the maximum CE peaks for (a) F_2, (b) F_3, (c) F_4, results were calculated for $\theta = 6^\circ$, $\theta = 10^\circ$, and $\theta = 14^\circ$, respectively. The waveguide thickness was 220 nm. Different etch-depths were used for each Fibonacci step: (a) 70 nm, (b) 140 nm, and (c) 140 nm.

the grating coupler could be an alternative to reduce reflections. However, this approach can be challenging because the required featured sizes may be beyond the limit of standard fabrication tools [33]. Calculations for F_5, not shown here, were performed using 6 *ABAABABA* periods with maximum CEs around 20%, which may be due to the small amount of periods, i.e., due to the lack of long-range periodicity we cannot expect an efficient phase-matching between the grating and waveguide modes.

Field profiles of E_y are shown in Figures 8(a)-(c) for the maximum CE peaks of F_2, F_3, and F_4, respectively. Calculations were made using different θ, etch-depth, wavelength and grating coupler lengths, according to results in Figures 5 to 7. More specifically, we used $\theta = 6^\circ$, $\mathrm{etch-depth} =$ 70 nm, and $\lambda = 1579$ nm for F_2. In the calculation for F_3 and F_4 we used $\mathrm{etch-depth} = 140$ nm for both systems, whereas θ (λ) were used as 10° (1188 nm) and 14° (1631 nm), respectively. Reflections at the grating-fiber interface for Figures 8(a)-(c) were approximately 10%, 20% and 10%, respectively. Low efficiency amplitudes are thus mainly due to the light guided in the glass below the Si waveguide, as it can also be noted from the corresponding **Visualization** files.

IV. Discussion and Conclusion

We have demonstrated numerically that a single structure - quasiperiodic grating coupler - is capable of multiple wavelength fiber-waveguide coupling. Results were obtained for fiber modes with wavelengths ranging from 1.0 μm to 2.0 μm, but they can be extended to wider or higher wavelength ranges. Our concept uses fractal unit cells built according, but not limited to, the Fibonacci sequence. Multiple peaks in the CE spectrum are due to the increased number of allowed modes in these platforms, as observed in analogous studies. Significantly, overlapping multiple CE peaks (through proper engineering) could be used as a way to produce ultra-broadband fiber-waveguide coupling, which still remains as one of the major problems in this area. We must remark that all the structures in this work used a waveguide thickness of 220 nm, which could not be the optimum value. Thus, we expect that this seminal work stimulates further investigation to produce multiple high efficiency peaks within a desired frequency range.

References

[1] J. Wang *et al.*, "Multidimensional quantum entanglement with large-scale integrated optics," *Science*, vol. 360, pp. 285–291, 2018.

[2] A. H. Atabaki *et al.*, "Integrating photonics with silicon nanoelectronics for the next generation of systems on a chip," *Nature*, vol. 556, pp. 349–354, 2018.

[3] D. Taillaert *et al.*, "Grating couplers for coupling between optical fibers and nanophotonic waveguides," *Jap. J. Appl. Phys.*, vol. 45, 2006, Art. no. 6071.

[4] X. Chen, K. Xu, Z. Cheng, C. K. Y. Fung, and H. K. Tsang, "Wideband subwavelength gratings for coupling between silicon-on-insulator waveguides and optical fibers," *Opt. Lett.*, vol. 37, 2012, Art. no. 3483.

[5] Q. Zhong *et al.*, "Focusing-curved subwavelength grating couplers for ultra-broadband silicon photonics optical interfaces," *Opt. Express*, vol. 22, 2014, Art. no. 18224.

[6] P. Cheben *et al.*, "Broadband polarization independent nanophotonic coupler for silicon waveguides with ultra-high efficiency," *Opt. Express*, vol. 23, 2015, Art. no. 22553.

[7] W. Z., Z. Cheng, X. Sun, and H. K. Tsang, "Tailorable dual-wavelength-band coupling in a transverse-electric-mode focusing subwavelength grating coupler," *Opt. Lett.*, vol. 43, pp. 2985–2988, 2018.

[8] J. Cao, F. Qi, S. Yan, and L. Zhang, "Highly-efficient three-dimensional waveguide coupler using impedance-tunable transformation optics," *Sci. Rep.*, vol. 8, 2018, Art. no. 9091.

[9] W. Zhou and H. K. Tsang, "Dual-wavelength-band subwavelength grating coupler operating in the near infrared and extended shortwave infrared," *Opt. Lett.*, vol. 44, pp. 3621–3624, 2019.

[10] T. Suhara and H. Nishihara, "Integrated optics components and devices using periodic structures," *IEEE J. Quant. Elect.*, vol. 22, no. 6, pp. 845–867, Jun. 1986.

[11] S. Lardenois *et al.*, "Low-loss submicrometer silicon-on-insulator rib waveguides and corner mirrors," *Opt. Lett.*, vol. 28, 2003, Art. no. 1150.

[12] L. Zhu, W. Yang, and C. Chang-Hasnain, "Very high efficiency optical coupler for silicon nanophotonic waveguide and single mode optical fiber," *Opt. Express*, vol. 25, 2017, Art. no. 18462.

[13] R. Marchetti *et al.*, "High-efficiency grating-couplers: Demonstration of a new design strategy," *Sci. Rep.*, vol. 7, 2017, Art. no. 16670.

[14] L. Su, R. Trivedi, N. V. Sapra, A. Y. Piggot, D. Vercruysse, and J. Vučković, "Fully-automated optimization of grating couplers," *Opt. Express*, vol. 26, 2018, Art. no. 4023.

[15] S. Nambiar, P. Sethi, and S. K. Selvaraja, "Grating-assisted fiber to chip coupling for SOI photonic circuits," *Appl. Sci.*, vol. 8, 2018, Art. no. 1142.

[16] E. W. Ong, T. Wallner, N. M. Fahrenkopf, and D. D. Coolbaugh, "High positional freedom SOI subwavelength grating coupler (SWG) for 300 mm foundry fabrication," *Opt. Express*, vol. 26, 2018, Art. no. 28773.

[17] N. Chen *et al.*, "Efficient and broadband subwavelength grating coupler for 3.7 μm mid-infrared silicon photonics integration," *Opt. Express*, vol. 26, 2018, Art. no. 26242.

[18] D. Benedikovic *et al.*, "Sub-decibel silicon grating couplers based on *L*-shaped waveguides and engineered subwavelength metamaterials," *Opt. Express*, vol. 27, 2019, Art. no. 26239.

[19] N. Hoppe *et al.*, "Ultra-efficient Silicon-on-insulator grating couplers with backside metal mirrors," *IEEE J. Sel. Topics Quantum Electron.*, vol. 26, no. 2, Mar./Apr. 2020, Art. no. 8200206.

[20] P. P. Absil *et al.*, "Silicon photonics integrated circuits: A manufacturing platform for high density, low power optical I/O's," *Opt. Express*, vol. 23, 2015, Art. no. 9369.

[21] D. Garcia-Rodriguez, J. L. Corral, A. Griol, and R. Llorente, "Bimodal grating coupler design on SOI technology for mode division multiplexing at 1550 nm," *Opt. Express*, vol. 26, 2018, Art. no. 19445.

[22] N. V. Sapra *et al.*, "Inverse design and demonstration of broadband grating couplers," *IEEE J. Sel. Topics Quantum Electron.*, vol. 25, no. 3, May/Jun. 2019, Art no. 6100207.

[23] E. R. Martins, J. Li, Y. K. Liu, J. Zhou, and T. F. Krauss, "Engineering gratings for light trapping in photovoltaics: The supercell concept," *Phys. Rev. B*, vol. 86, 2012, Art. no. 041404.

[24] S.-N. Zhu, Y.-Y. Zhu, Y.-Q. Qin, H.-F. Wang, C.-Z. Ge, and N.-B. Ming, "Experimental realization of second harmonic generation in a fibonacci optical superlattice of $LiTaO_3$," *Phys. Rev. Lett.*, vol. 78, 1997, Art. no. 2752.

[25] N. M. Lučić *et al.*, "Light propagation in quasi-periodic fibonacci waveguide arrays," *J. Opt. Soc. Am. B*, vol. 32, 2015, Art. no. 1510.
[26] F. Reyes Gómez, N. Porras-Montenegro, O. N. Oliveira Jr, and J. R. Mejía-Salazar, "Second harmonic generation in the plasmon-polariton gap of quasiperiodic metamaterial photonic superlattices," *Phys. Rev. B*, vol. 98, 2018, Art. no. 075406.
[27] A. N. Kalish *et al.*, "Magnetoplasmonic quasicrystals," *Optica*, vol. 5, pp. 617–623, 2018.
[28] E. Reyes-Gómez, N. Raigoza, S. B. Calvacanti, C. A. A. de Carvalho, and L. E. Oliveira, "Plasmon polaritons in photonic metamaterial Fibonacci superlattices," *Phys. Rev. B*, vol. 81, 2010, Art. no. 153101.
[29] L. Chrostowski and M. Hochberg, *Silicon Photonics Design: from Devices to Systems*. Cambridge, U.K.: Cambridge Univ. Press, 2015, pp. 162–181.
[30] K. A. Bates, L. Li, R. L. Roncone, and J. J. Burke, "Gaussian beams from variable groove depth grating couplers in planar waveguides," *Appl. Opt.*, vol. 32, 1993, Art. no. 2112.
[31] S. L. Chuang, *Physics of Photonic Devices*. 2nd ed. Hoboken, NJ, USA: Wiley, 2009, pp. 257–307.
[32] A. Bozzola, L. Carroll, D. Gerace, I. Cristiani, and L. C. Andreani, "Optimising apodized grating couplers in a pure SOI platform to -0.5 dB coupling efficiency," *Opt. Express*, vol. 23, 2015, Art. no. 16289.
[33] D. Vermeleun *et al.*, "High-efficiency fiber-to-chip grating couplers realized using an advanced CMOS-compatible Silicon-On-Insulator platform," *Opt. Express*, vol. 18, 2010, Art. no. 18278.